Molecular dynamics simulations of point defects in plutonium grain boundaries*

Ao Bing-Yun(敖冰云)[a)†], Xia Ji-Xing(夏吉星)[b)], Chen Pi-Heng(陈丕恒)[a)], Hu Wang-Yu(胡望宇)[b)], and Wang Xiao-Lin(汪小琳)[a)]

[a)] *National Key Laboratory for Surface Physics and Chemistry, P. O. Box* 718–35, *Mianyang* 621907, *China*

[b)] *Department of Applied Physics, Hunan University, Changsha* 410082, *China*

(Received 17 May 2011; revised manuscript received 21 August 2011)

A modified analytic embedded atom method (MAEAM) potential is constructed for fcc δ-Pu. Molecular dynamics (MD) simulations with the potential are performed to investigate the interactions between two symmetrical tilt grain boundaries (GBs) and point defects such as He atom, vacancy and self-interstitial atom (SIA) in Pu. The calculated results show that point defect formation energies are on average lower than those in the lattice but variations from site to site along the GBs are very remarkable. Both substitutional and interstitial He atoms are trapped at GBs. Interstitial He atom is more strongly bound at the GB core than the substitutional He atom. The binding energy of SIA at GB core is higher than those of He atom and vacancy. GB core can bind many He atoms and SIAs due mainly to the fact that it contains many vacancies. Compared with He atom and SIA, the vacancy far from GB core is difficult to diffuse into the core. The GBs can act as sinks and sources of He atoms and SIAs, which may be a reason for the swelling of Pu after a period of self-irradiation because of the higher concentration of vacancy in the bulk.

Keywords: plutonium, molecular dynamics, crystal defect, radiation damage

PACS: 61.72.–y, 61.72.Cc, 61.72.Qq, 71.15.Pd **DOI:** 10.1088/1674-1056/21/2/026103

1. Introduction

Pu is perhaps the most complex metallic element, owing to seven known crystal structures of metallic Pu existing between very low temperature and relatively low melting point (913 K) and has attracted extraordinary scientific interest since its discovery in 1941. Among all the different Pu crystal structures, δ-Pu is the most technologically important because it is ductile and malleable (the ground state Pu is hard and brittle) and can be stabilized at room temperature when alloyed with a few atomic percent of impurities such as Ga and Al. Thus it becomes the most studied phase. However, modern-day problems concerning Pu involve understanding and predicting the properties of Pu and its alloys for the safe handling, use and long-term storage of these important but highly toxic materials which made experimental observations extremely difficult.[1] So, development of a predictive aging model for Pu is one of major goals of many researchers' studies on Pu.

Pu is vulnerable to aging because it is a radioactive element, decaying to U by emitting the α particle. The 86-keV ^{235}U recoil traverses the lattice approximately 12 nm and results in the formation of approximately 2300 Frenkel pairs. Although 90% of these Frenkel pairs return to the initial lattice sites in the first 200 nanoseconds, the remaining 10% remain in the lattice in the form of free self-interstitial atoms (SIAs) and vacancies or SIA or vacancy clusters. On the other side of the α decay, a 5-MeV α particle traverses the lattice approximately 10 μm, slowly losing its energy via electronic excitations before coming to rest with the generation of an additional 265 Frenkel pairs. Although the widely used ^{239}Pu has a relatively long half-life of about 2.4×10^4 years, its decay rate is still sufficiently high to lead to a significant buildup of He and radiation damage within the metal after several decades.[2] As is well known, He and radiation damage in metals can produce macroscopic detrimental effects such as swelling and embrittlement, thus alter the properties of metals and alloys. Beyond all doubt, Pu and its alloys must also be the very typical examples.

Despite some researches regarding He effects and radiation damage in Pu with direct and indirect tech-

*Project supported by the National Natural Science Foundation of China (Grant No. 20801007) and the Science and Technology Foundation of China Academy of Engineering Physics (Grant No. 2009A0301019).

†Corresponding author. E-mail: aobingyun24@yahoo.com.cn

© 2012 Chinese Physical Society and IOP Publishing Ltd

niques, many questions remain unsolved,[3,4] especially concerning the intrinsic behaviours of point defects (vacancy, SIA and impurities) and extended defects (GB, dislocation, void, bubble, etc.) and the influence of these defects on the properties of Pu. In order to obtain further knowledge about the behaviours of defects in Pu, malecular dynamics (MD) simulations are performed to investigate these problems. However, the discussion on displacement cascades such as defects evolution in Pu is beyond the scope of this paper. In our previous work, the behaviours of He-vacancy clusters were studied. The results showed that the binding energies of He atom, vacancy and SIA in He-vacancy cluster depend mainly on the He-vacancy atomic ratio rather than the clusters size. He atom and SIA can stabilize He-vacancy cluster to a rather high critical He density until a new SIA is produced because of very high He pressure in the cluster, in the meantime, it is very difficult for vacancy to detrap from the cluster.[5,6] In the present paper we extend our previous work by using the same computational methods to research the interactions between point defects and the symmetrical tilt GBs which are commonly regarded as an important kind of defect in Pu.

The rest of the present paper is organized as follows. In Section 2, we outline the procedure of simulations and describe the potentials used in the present work. The calculations are discussed in Section 3. Conclusive comments are provided in Section 4.

2. Method of calculations

2.1. Molecular dynamics

A complete understanding of the behaviours of defects in Pu requires an atomic-level computer simulation. MD simulation is an important tool for understanding materials at atomic level. By using MD simulation, the behaviours of defects in solid materials can be directly probed. The general methods of MD simulation have been discussed in great details by a number of authors; thus, we give here only the specific details of our calculations. In the present MD simulation, the six-value Gear predictor–corrector algorithm and Nosé constant-temperature technique[7] with a time step of 1 fs are employed. Usually, the total simulation time is 100 ps, but in some cases, for instance the computational system contains a great number of defects, the total simulation time is high to 5 ns, depending on the computational cell being simulated. The thermodynamic quantities are evaluated only after ensuring a thorough equilibration of the computational system.

2.2. Potentials

The success of the MD simulation lies in the choices of the interatomic potentials of Pu–Pu and Pu–He. We have developed our own Pu–Pu embedded atom method (EAM) potential to reproduce the fcc δ-Pu and Pu–He Morse pair potential.[5,6] In the original EAM model, there are two assumptions.[8] First, the atomic electron densities are to be well represented by the spherically averaged free atom densities calculated from Hartree–Fock theory. Second, the host electron density is approximated by a linear superposition of the atomic densities of the constituents. These assumptions are too simple and cannot describe the actual situation well. Baskes[9] modified it to include direct bonding in the expression of electron density and applied it to a variety of cubic materials, but the calculations were very complicated. Our group[10] proposed another modified method. With introducing a modified energy term $M(P)$ into the total energy expression to express the energy difference resulting from the electron density difference and to correct the negative Cauchy relation, a new type of modified analytic EAM (MAEAM) has been constructed for almost all typical metals.[11−15]

The present MAEAM describes the total energy $E_{\rm t}$ of any structure as the sum of three terms: a many-body term depending on the local electron density, a two-body term depending on interatomic distances and a modification term to correct the assumption of the linear superposition of atomic electron density in the original EAM,

$$E_{\rm t} = \sum_i F(\rho_i) + \frac{1}{2}\sum_{i,j}\phi(r_{ij}) + \sum_i M(P_i) \quad \text{for} \quad i \neq j, \tag{1}$$

where $\phi(r)$ is the effective two-body potential, $F(\rho)$ is the embedding energy. The local electron density ρ_i and its second order P_i are determined by a superposition of individual atomic electron densities $f(r_{ij})$, respectively, as

$$\rho = \sum_m f(r_m), \tag{2}$$

$$P = \sum_m f^2(r_m), \tag{3}$$

where m is the number of the neighbour atoms. The

atomic electron density is described by function $f(r)$,

$$f(r) = \left(\frac{r_1}{r}\right)^{4.7} \left[\frac{r_{\rm ce} - r}{r_{\rm ce} - r_1}\right]^2, \quad (4)$$

where r_1 is the nearest neighbour atomic equilibrium distance, $f(r)$ is truncated at $r_{\rm ce}$, $r_{\rm ce} = r_4 + 0.75(r_5 - r_4)$, with r_4 and r_5 being the fourth and fifth neighbour distances for a perfect crystal, respectively.

The energy modification term is empirically taken as

$$M(P) = \alpha \left\{1 - \exp\left[-10^4 \left(\ln\left(\frac{P}{P_{\rm e}}\right)\right)^2\right]\right\}, \quad (5)$$

where $P_{\rm e}$ is its equilibrium value.

The embedding function of $F(\rho)$ takes the same form as that used by Johnson,[16] i.e.,

$$F(\rho) = -F_0 \left[1 - n\left(\ln\frac{\rho}{\rho_{\rm e}}\right)\right] \left(\frac{\rho}{\rho_{\rm e}}\right)^n, \quad (6)$$

where F_0 and n are model parameters and $\rho_{\rm e}$ is the equilibrium electron density.

A Morse-like pair potential is proposed in the frame of our MAEAM. The proposed pair potential $\phi(r)$ is

$$\begin{aligned}\phi(r) = {} & k_0 + k_1 \exp\left(1 - \frac{r}{r_1}\right) + k_2 \exp\left[2\left(1 - \frac{r}{r_1}\right)\right] \\ & + k_3 \exp\left[3\left(1 - \frac{r}{r_1}\right)\right] + k_4 \exp\left[4\left(1 - \frac{r}{r_1}\right)\right] \\ & + k_{-1} \exp\left(\frac{r_1}{r} - 1\right), \end{aligned} \quad (7)$$

where k_i ($i = -1$, 0, 1, 2, 3 and 4) are the potential parameters. In the present model, the atomic interactions up to the third neighbour distance are considered and $\phi(r)$ is truncated between the third and the fourth neighbour distance, $r_{\rm c} = r_3 + 0.75(r_4 - r_3)$. At this point, the pair potential and its slope are zero, i.e.

$$\phi(r_{\rm c}) = 0, \quad \phi'(r_{\rm c}) = 0. \quad (8)$$

All the model parameters are determined analytically by fitting the properties of metals, such as lattice constants a, cohesive energy $E_{\rm c}$, mono-vacancy formation energy $E_{1\rm f}$ and elastic constants C_{11}, C_{12}, C_{44}. The input physical parameters for Pu are listed in Table 1.[17–19] Although this potential is for pure Pu, the elastic constants and the mono-vacancy formation energy are taken from a Ga-stabilized Pu δ-alloy (fcc crystal structure). The Pu EAM potential has proven to be effective to a certain extent to reproduce many properties of Pu, but it can reproduce neither the complicated phase transformations nor the unusual phonon softening in δ-Pu.[18,20–23] In fact, many of these difficulties can be overcome only by the most advanced electronic structure calculation methods, for example, the recently developed dynamics mean-field theory (DMFT) has been succeeded in reproducing the unusual phonon softening in δ-Pu.[19,24–26] From the viewpoint of atomic-level computer simulation, the Pu MAEAM potential can be tentatively used to investigate the atomic behaviour of defects in Pu.

Table 1. Input physical parameters for the δ-Pu MAEAM potential, a is the lattice constant, $E_{\rm c}$ the cohesive energy, $E_{1\rm f}$ the mono-vacancy formation energy and C_{11}, C_{12}, and C_{44} are the elastic constants.

a/nm	$E_{\rm c}$/eV	$E_{1\rm f}$/eV	C_{11}/GPa	C_{12}/GPa	C_{44}/GPa
0.464	4.2	0.9	38.0	26.0	33.0

The He–He potential used is the Lennard–Jones pair potential,[27]

$$\phi = \phi_0 \left[\left(\frac{r_0}{r}\right)^{12} - 2\left(\frac{r_0}{r}\right)^6\right], \quad (9)$$

where ϕ_0 and r_0 are the potential parameters. The He–He potential has been widely used to study He effects in solid materials.

For the Pu–He cross potential, there is no experimental data at all with which to fit the potential. As is well known, He atom has a filled-shell electronic configuration and is thus likely to interact with other atoms in a simpler way than metal atoms, in other words, the electronic effects of He-metals interactions may be negligible. For this reason, the Pu–He cross potential was modeled as Morse pair potential,

$$\begin{aligned}\phi = {} & \phi_0 \Bigg[\exp\left(-2\alpha\left(\frac{r}{r_0} - 1\right)\right) \\ & - 2\exp\left(-\alpha\left(\frac{r}{r_0} - 1\right)\right)\Bigg], \end{aligned} \quad (10)$$

where ϕ_0, r_0, and α are the potential parameters. In order to determine the potential parameters, we try to compare Pu with other fcc metals (such as Al, Pd, and Ni) whose interaction potentials with He were developed by using first-principles calculations.[28] We have obtained the potential parameters by choosing from a variety of values of ϕ_0, r_0, and α. Although the fidelity of the potential parameters is limited, the Pu–He cross potential is qualitatively feasible for modeling the behaviour of He atoms in Pu. Furthermore, the selected potential parameters are in accordance with the Pu–He dimer potential developed by using *ab initio* calculations.[29,30]

2.3. Atomic structures of GBs

The interactions between point defects and GBs are investigated within the framework of coincidence site lattice (CSL). Coincidence boundaries are fundamental to current models of grain-boundary structure and, in addition, have a number of simplifying features from the computational standpoint. To describe a GB geometrically, a number of variables must be specified. In general, a GB has five macroscopic degrees of freedom. Three of them determine mutual rotational relationship of the two adjacent grains. The rotation that would lead to a perfect matching of crystal lattices of both grains is determined by the rotation axis $\bar{o}$ and by the angle θ describing the misorientation of the grains. The misorientation of a GB is given by the normal $\bar{n}$ to the grain GB.

According to the relationship between the rotation axis and the normal to the boundary plane, GB are categorized as tilt ($\bar{o} \perp \bar{n}$), twist ($\bar{o} \parallel \bar{n}$), and mixed. According to the misorientation angle θ of the grains, low angle ($\theta < 15°$) and high ($\theta > 15°$) are usually defined. When the GB plane represents the mirror symmetry plane of crystal of both adjacent grains, the boundary is called symmetrical, in all other cases it is called asymmetrical. In a cubic system the symmetrical tilt GB on the (310) type planes of both adjacent grains characterized by the misorientation angle ($\theta = 36.87°$) along the common rotation axis [001] is denoted as 36.87° (310)[001] symmetrical tilt GB.

For a given misorientation θ, the CSL is a superlattice that may be constructed by coinciding with atom positions of the crystal lattices of both adjacent grains when they are extrapolated across the boundary to interpenetrate each other. The reciprocal density of CSL is denoted by Σ and is often used as a geometric parameter characterizing the structure-property relationship. For cubic crystal, Σ can be determined by

$$\Sigma = \delta\left(h^2 + k^2 + l^2\right), \tag{11}$$

where h, k and l are the Miller indices of the symmetrical tilt GB corresponding to the given misorientation θ. The parameter $\delta = 1$ if $h^2 + k^2 + l^2$ is odd and $\delta = 0.5$ if $h^2 + k^2 + l^2$ is even.[31−33]

We first consider the structures of two symmetrical tilt GBs, i.e. $\Sigma5(310)[001]$ and $\Sigma5(210)[001]$, with misorientation angles: 36.87° and 53.13°, which are well known from experimental observations and computational simulations.[31−33] The unrelaxed ground state structures of two GBs are shown in Figs. 1(a) and 1(b). In our simulations, GBs $\Sigma5(310)[001]$ and $\Sigma5(210)[001]$ contain 3600 and 5000 Pu atoms, respectively. In order to obtain the equilibrium structures of two GBs, annealing MD is employed and periodic boundary conditions are imposed in the direction parallel to the GB plane. Each GB contains free atoms, which are able to move under interatomic forces and fixed atoms which are fixed at their lattice sites to maintain the total volume of the computational system. The computational systems are relaxed at 300 K, with the temperature controlled via explicit rescaling of the velocities and the pressure controlled using Parrinello and Rahman method,[34] followed by slowly cooling and quenching the systems to 0 K. The positions of the atoms are relaxed to their minimum energy configurations. The point defects are placed at different sites along GBs. After static relaxation, the point defect formation energy can be determined by comparing the energy of GB containing a point defect with that of the same-size GB without point defect.

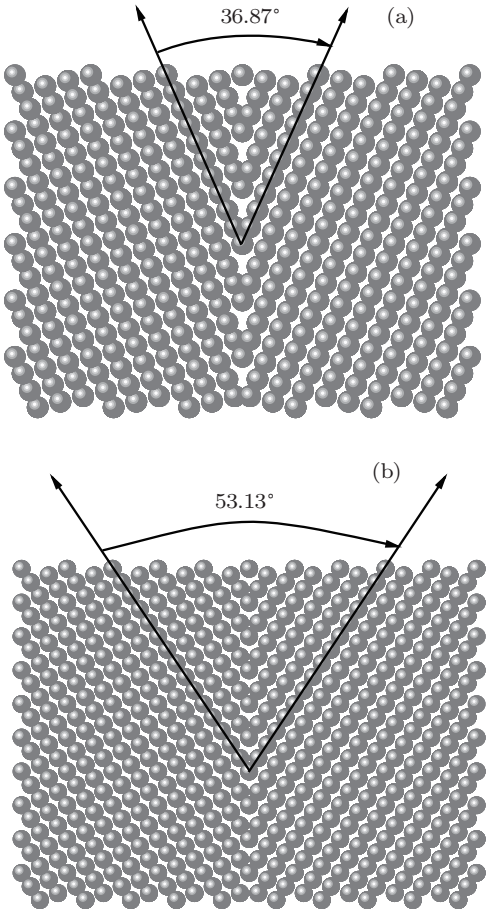


Fig. 1. Initial atomic structures of two symmetrical tilt GBs. (a) $\Sigma5(310)[001]$–36.87°, (b) $\Sigma5(210)[001]$–53.13°.

3. Results and discussion

3.1. Interactions between He atom and GBs

It is well known that He atom in metal initially occupies an interstitial site with a high mobility before becoming deeply trapped in other defect such as a radiation or thermal vacancy. In this case, a substitutional He atom is formed. The interactions between He atom and GBs are investigated by the insertion of a single He atom at either an interstitial or a substitutional (replacement of a Pu atom with an He atom) location along GBs, thereby relaxing the computational system. The formation energy of the He atom (either interstitial or substitutional) at a particular site α along GB is determined from the following equation:

$$E_{\rm f}^{\alpha}({\rm He}) = E_{\rm c}^{\alpha}({\rm GB}) - E_{\rm c}({\rm GB}) - \varepsilon({\rm He}), \qquad (12)$$

where $E_{\rm c}^{\alpha}({\rm GB})$ and $E_{\rm c}({\rm GB})$ are the total configuration energies of the relaxed GB with an He atom at site α and without the He atom, respectively and $\varepsilon({\rm He})$ is the cohesive energy of a perfect fcc He crystal. Here, the calculated cohesive energy of perfect crystal is -0.0071 eV/atom for He. The strength of the interaction between a point defect and a GB is represented by its binding energy. The binding energy of the He atom at the site α to the GB core is calculated from the following equation:

$$E_{\rm b}^{\alpha}({\rm He}) = E_{\rm f}({\rm He}) - E_{\rm f}^{\alpha}({\rm He}), \qquad (13)$$

where $E_{\rm f}({\rm He})$ is the formation energy of He atom (either interstitial or substitutional) in the perfect Pu crystal. The calculated values are 2.3 eV and 1.53 eV for interstitial and substitutional He atoms, respectively.

In Figs. 2 and 3, the formation energy and the binding energy of interstitial and substitutional He atoms each are plotted as a function of the distance from GB core. The results show that the formation energies are lower than in the perfect crystal but variations from site to site along GBs are very remarkable. Both substitutional and interstitial He atoms are trapped at GBs, a result that is similar to the findings of Baskes and Vitek in fcc Ni,[35] and Kurtz and Heinisch in bcc Fe.[36] Interstitial He atom is much more strongly bound at GB core than substitutional He atom (He-vacancy complex), owing mainly to the strong binding of the He atom to vacancy. It is clear that the binding energy of an He atom at GB core is greater than that of an He atom to vacancy by a few tenth of an electronvolt. As a result of its filled-shell electronic configuration, He atom energetically prefers to occupy the site with low electron density like vacancy, void, dislocation, and GB. After relaxation, GB contains a certain concentration of vacancies or vacancy-like defects, which may explain the relatively high binding energy of He atom at GB core. The binding energies for both interstitial and substitutional He atoms are close to zero at some distances. For the GB $\Sigma5(310)[001]$, the distances from the GB core, i.e., capture radii, are about 9.2 Å (1 Å=0.1 nm) and 4.2 Å for interstitial and substitutional He atoms, respectively. For the GB $\Sigma5(210)[001]$, the corresponding capture radii are 9.2 Å and 6.5 Å, which implies that the capture radius depend on GB structure. Further work on the dependence of GB structure on binding He atom is in progress.

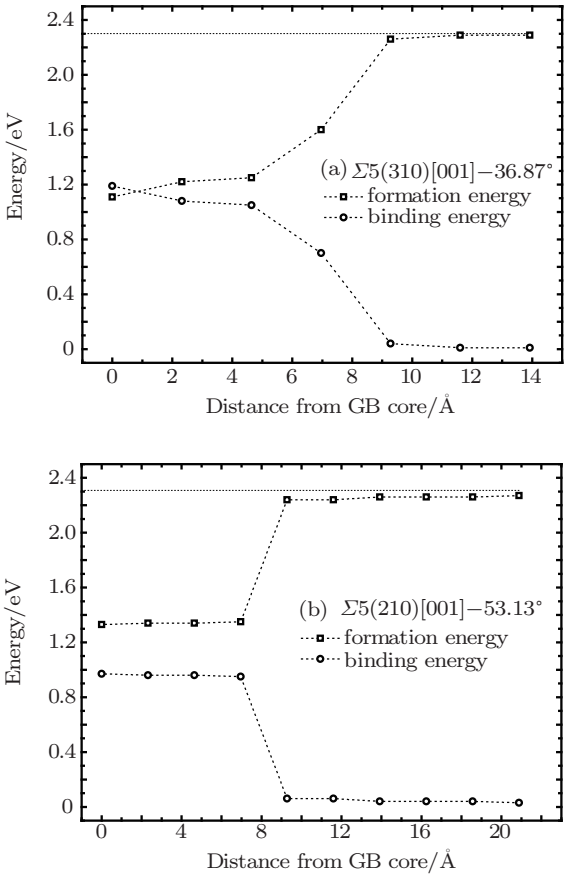


Fig. 2. Formation energies and binding energies of interstitial He atom each as a function of the distance from the GB core. (a) $\Sigma5(310)[001]$–36.87°, (b) $\Sigma5(210)[001]$–53.13°.

The high binding energy of the interstitial He atom at GB indicates that GB is a sink for trapping He atoms. The interactions between a few of He atoms and GB are investigated by adding He atoms one by one into GB core. The first He atom is introduced

into GB core for calculating the formation energy of single He atom. Afterwards, the second He atom is introduced at the nearest neighbour interstitial site of the first He atom for calculating the formation energies of two He atoms and the second He atom. In this way, 20 He atoms are sequentially introduced into GB core.

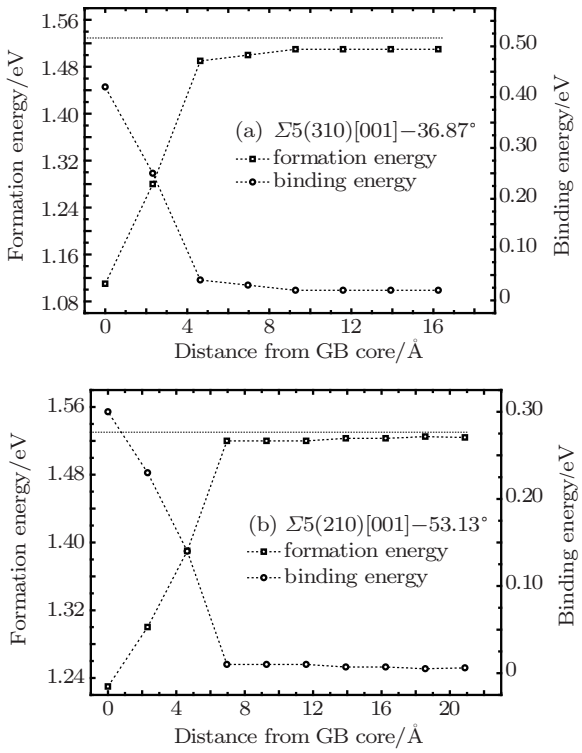


Fig. 3. Formation energies and binding energies of substitutional He atom each as a function of the distance from the GB core. (a) $\Sigma5(310)[001]$–36.87°, (b) $\Sigma5(210)[001]$–53.13°.

Figures 4(a) and 4(b) show the plots of the average formation energy of He atom and the formation energy of the n-th He atom at two GBs versus the number of He atoms. As shown in the two figures, the average formation energy and the formation energy of the n-th He atom at two GBs slowly decrease with the increase of the number of He atoms. The results also imply that the average binding energy and the binding energy of the n-th He atom at two GBs slowly increase with the increase of the number of He atoms, which shows that the ability to trap He atom for GB increases with the increase of the number of He atoms, a result that is similar to the experimental result given by Kimura *et al.* in martensitic steels.[37] From these results, we can conclude that He atoms tend to form bubbles in the GB core. The conclusion is likely to provide perception in understanding He embrittlement or He damage in Pu. Researches concerning this problem focus on He diffusion along GBs.

The diffusion coefficient D can be calculated from the jump-frequency method. On the other hand, we know the Arrhenius relation as follows:

$$\ln D = \ln D_0 - \frac{E_\mathrm{a}}{k_\mathrm{B} T}, \tag{14}$$

where E_a is the activation energy for He atom diffusion. Comparative investigations on He diffusion in perfect lattice and along GBs in Pu have shown that He atom diffusion along GBs is faster than in perfect lattice, which may lead to a rapid accumulation of He atoms in GBs resulting in the formation of bubbles. Figures 5(a) and 5(b) show the typical He diffusion trajectory along GB and the plot of $\ln D$ versus $1/T$, respectively. He diffusion along GBs has the obvious two-dimensional characteristic whereas He diffusion in perfect lattice has the random-jump three-dimensional characteristic. The activation energies for He atom diffusion along GBs $\Sigma5(310)[001]$

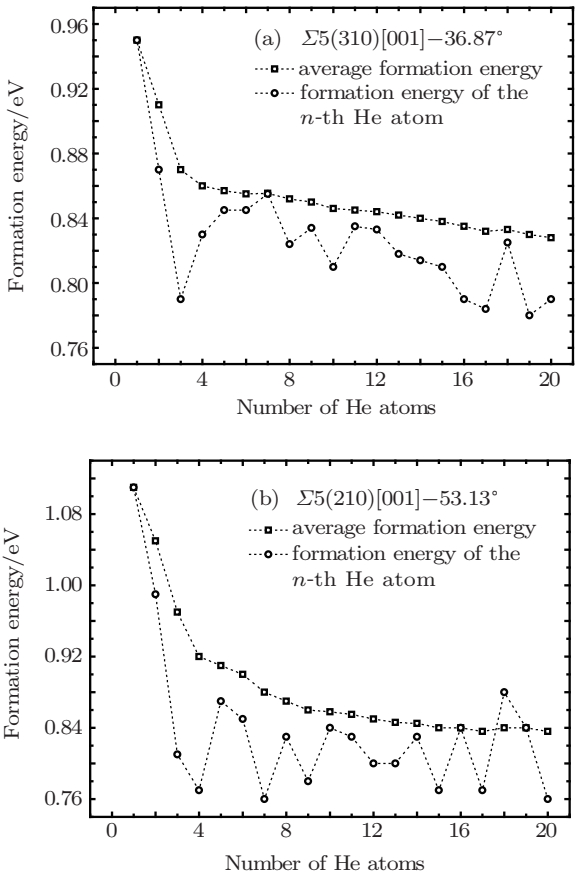


Fig. 4. Formation energies of multiple He atoms each as a function of the number of He atom. (a) $\Sigma5(310)[001]$–36.87°, (b) $\Sigma5(210)[001]$–53.13°.

and $\Sigma5(210)[001]$ are evaluated to be 0.086 eV and 0.12 eV, respectively, which are lower than the activation energy for He atom diffusion in perfect lattice ($E_\mathrm{a} = 0.22$ eV). Interestingly, the activation energies

for He diffusion along GBs and in perfect lattice are lower than those for the He diffusion in other fcc and bcc metals, which may illuminate the rapid nucleation and the formation of He bubble in Pu.

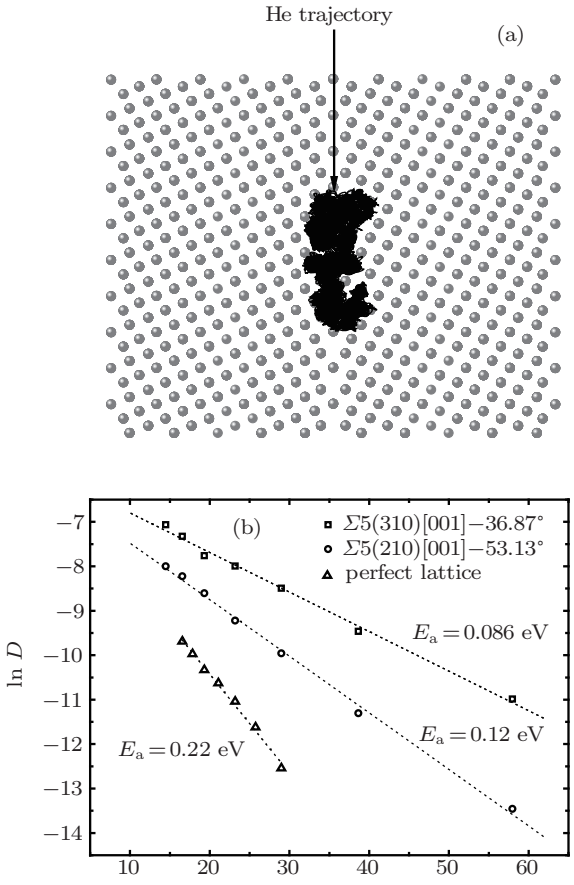


Fig. 5. He diffusion along GBs. (a) Typical He diffusion trajectory, (b) the plot of ln$D$ versus $1/T$. The calculation result of He diffusion in perfect lattice is shown for comparison.

3.2. Interactions between vacancy and GBs

The formation energy of vacancy at a particular site β along GB is determined from the equation,

$$E_{\rm f}^{\beta}({\rm V}) = E_{\rm c}^{\beta}({\rm GB}) - E_{\rm c}({\rm GB}) + \frac{E_{\rm c}({\rm GB})}{N}, \quad (15)$$

where $E_{\rm c}^{\beta}({\rm GB})$ and $E_{\rm c}({\rm GB})$ are the total configuration energies of the relaxed GB with a vacancy at site β and without the vacancy, respectively, N is the number of Pu atoms of the initial GB. The vacancy binding energy is then given by

$$E_{\rm b}^{\beta}({\rm V}) = E_{\rm f}({\rm V}) - E_{\rm f}^{\beta}({\rm V}), \quad (16)$$

where $E_{\rm f}({\rm V})$ is the vacancy formation energy in the perfect Pu crystal and is chosen to be 0.9 eV in our EAM model. In Figs. 6(a) and 6(b), the vacancy formation energy and the vacancy binding energy each are plotted as a function of the distance from the GB core. As shown in the figures, the formation energies are lower than those in the perfect crystal but variations from site to site along the GBs are very significant. The vacancy capture radii are both about 4.2 Å for the two GBs which are smaller than those of He atom and SIA as discussed below. Most of vacancies studied are found to be well localized, with neighbour Pu atoms showing relatively small relaxation towards the vacancy sites compared with the cases of interstitial He atom and SIA.

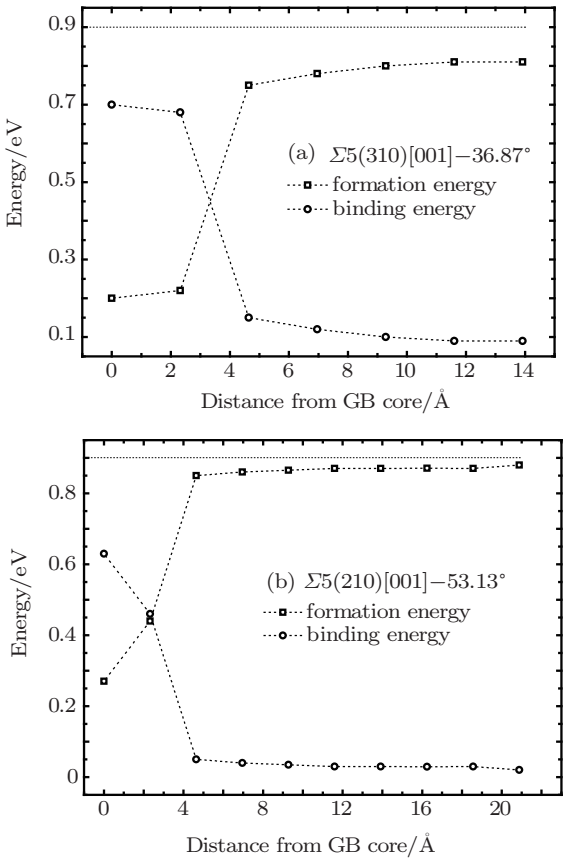


Fig. 6. Formation energies and binding energies of vacancy each as a function of the distance from the GB core. (a) $\Sigma5(310)[001]$–36.87°, (b) $\Sigma5(210)[001]$–53.13°.

The short vacancy capture radius means that it is difficult for vacancy to migrate from the bulk into the GB core. However, the vacancy formation energy near GB core is little lower than that in the bulk, which may explain the void swelling in the vicinity of GB. The initial numbers of vacancy and SIA generated by self-irradiation in the form of Frenkel pairs are equal. Due to the very low energy barrier for SIA migration and the high binding energy at GB, the rate of absorption of SIAs by GB (or other extended defects, no discussion in the paper) would be higher than the rate of absorption of vacancies. Those vacancies migrating in the vicinity of GB would cluster to form

void, which is also consistent with our previous findings, showing that the vacancy binding energy is little greater than zero even for the rather large void. As a matter of fact, void swelling in the vicinity of GB in many irradiated materials has been widely reported experimentally and theoretically.[38−40] Moreover, the void or the bubble swelling is one of the most concerns regarding the aging of Pu in long-term storage conditions. Our results may play a basic role in understanding this issue.

3.3. Interactions between SIA and GBs

The formation energy of an SIA at a particular site γ along GB is determined from the following equation:

$$E_{\rm f}^{\gamma}({\rm SIA}) = E_{\rm c}^{\gamma}({\rm GB}) - E_{\rm c}({\rm GB}) - \frac{E_{\rm c}({\rm GB})}{N}, \quad (17)$$

where $E_{\rm c}^{\gamma}({\rm GB})$ and $E_{\rm c}({\rm GB})$ are the total configuration energies of the GB with an SIA at site γ and without the SIA, respectively. The SIA binding energy is then determined by

$$E_{\rm b}^{\gamma}({\rm SIA}) = E_{\rm f}({\rm SIA}) - E_{\rm f}^{\gamma}({\rm SIA}), \quad (18)$$

where $E_{\rm f}({\rm SIA})$ is the SIA formation energy in the perfect Pu crystal and is calculated to be 2.3 eV. In Figs. 7(a) and 7(b), the SIA formation energy and the SIA binding energy are plotted each as a function of the distance from the GB core. As shown in the figures, the formation energies are greatly lower than those in the perfect crystal but variations from site to site along the GBs are also very remarkable. The SIA binding energy far from the GB core remains very high, which indicates that the SIA capture radius is much greater than those of He atom and vacancy.

In our simulations, the SIA is inserted into the GB core by simply putting a Pu atom at a pre-selected interstitial site and allowing the system to relax. Due to the high stress around the SIA, considerable relaxation occurs around the SIA and the relaxation configuration shows some delocalization, which forms a lower-energy configuration and may be the reason for the very low SIA formation energy. The observations from capture radius and binding energy show that GB can act as a deep sink to trap more SIAs than vacancies and thus provides the same support discussed in Subsection 3.2 that Pu would swell after a period of self-irradiation due mainly to the higher concentration of vacancies in the bulk or in the vicinity of GB. In addition, as the binding energies of He atom and SIA to vacancy are comparable to those at GB core, the strong binding of interstitial He atom and SIA at GB core may be induced by relatively high concentration of vacancies at GB core. From the viewpoint of energy, both interstitial He atom and SIA preferentially stay at GB rather than remain at the lattice if the temperature of the computational system is high enough for interstitial He atom and SIA to jump over their relatively low energy barriers.

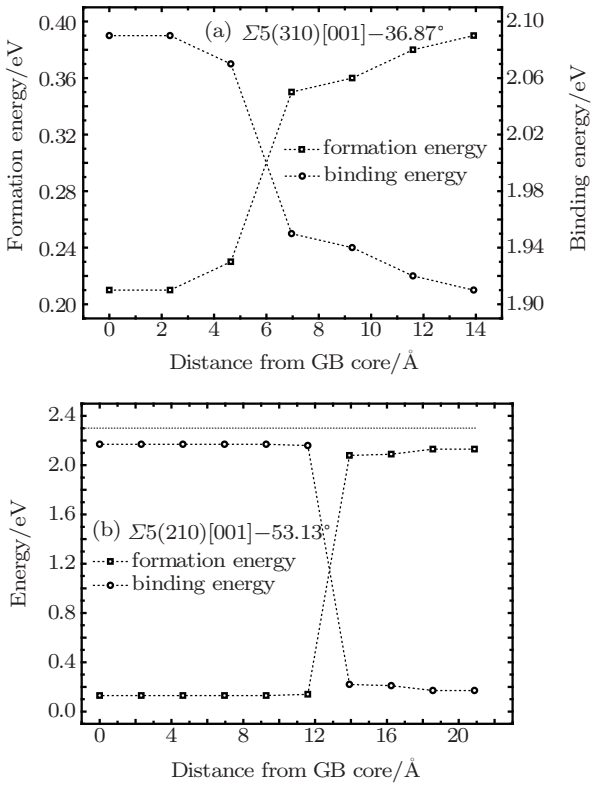


Fig. 7. Formation energies and binding energies of SIA each as a function of the distance from the GB core. (a) $\Sigma5(310)[001]$–36.87°, (b) $\Sigma5(210)[001]$–53.13°.

4. Conclusion

A computational framework based on MD simulations and EAM potential to investigate the interactions between point defects and two symmetrical tilt GBs in δ-Pu is presented. GBs can act as sinks for point defects especially for interstitial He atom and SIA. The results indicate that the GBs give rise to zone energetically more favourable for the interstitial He atom and SIA accumulation than for vacancy accumulation. In addition, the observations show that GB core can bind many interstitial He atoms which will cluster and finally form He bubble. GB does certainly determine the role and the extent of the migration and diffusion of point defects. Our calculations show in general good agreement with other authors' reports

for various GB structures in other fcc metals. However, as the extraordinary complexity of the crystal defect structure of Pu due to its self-irradiation effects, more work on the behaviours of various defects is under way.

References

[1] Chen J, Meng D Q, Du J G, Jiang G, Gao T and Zhu Z H 2010 *Acta Phys. Sin.* **59** 1658 (in Chinese)

[2] Wolfer W G 2000 *Los Almos Sci.* **26** p. 274

[3] Ao B Y, Wang X L, Chen P H, Shi P, Hu W Y and Yang J Y 2010 *Acta Phys. Sin.* **59** 4818 (in Chinese)

[4] Wu H L, Tian D F, Hao F H and Gong J 2011 *Acta Phys. Sin.* **60** 032801 (in Chinese)

[5] Ao B Y, Wang X L, Hu W Y, Yang J Y and Xia J X 2007 *J. Alloys Compd.* **444–445** 300

[6] Ao B Y, Yang J Y, Xia J X, Wang X L and Hu W Y 2009 *J. Nucl. Mater.* **385** 75

[7] Nosé S 1991 *Prog. Theor. Phys. Suppl.* **103** 1

[8] Daw M S and Baskes M I 1984 *Phys. Rev.* B **29** 6443

[9] Baskes M I 1992 *Phys. Rev.* B **46** 2727

[10] Ouyang Y, Zhang B, Liao S and Jin Z 1996 *Z. Phys.* B **101** 161

[11] Deng H, Hu W, Shu X and Zhang B 2003 *Surf. Sci.* **543** 95

[12] Yang J, Hu W, Deng H and Zhao D 2004 *Surf. Sci.* **572** 439

[13] Hu W, Zhang B, Huang B, Gao F and Bacon D J 2001 *J. Phys.: Condens. Matter* **13** 1193

[14] Hu W, Deng H and Fukumoto M 2003 *Eur. Phys. J.* B **34** 429

[15] Hu W, Shu X and Zhang B 2002 *Comput. Mater. Sci.* **23** 175

[16] Johnson R A 1990 *Phys. Rev.* B **41** 9717

[17] Pochet P 2003 *Nucl. Instr. Method Phys. Res.* B **202** 82

[18] Baskes M I 2000 *Phys. Rev.* B **62** 15532

[19] Dai X, Savrasov S Y, Kotliar G, Migliori A, Ledbetter H and Abrahams E 2003 *Science* **300** 953

[20] Cherne F J, Baskes M I and Holian B L 2003 *Phys. Rev.* B **67** 092104

[21] Valone S M, Baskes M I, Stan M, Mitchell T E, Lawson A C and Sickafus K E 2004 *J. Nucl. Mater.* **324** 41

[22] Fluss M J, Wirth B D, Wall M, Felter T E, Caturla M J, Kubota A and de la Rubia T D 2004 *J. Alloys Compd.* **368** 62

[23] Baskes M I, Muralidharan K, Stan M, Valone S M and Cherne F J 2003 *JOM* **9** 41

[24] Wong J, Krisch M, Farber D L, Occelli F, Schwartz A J, Chiang T C, Wall M, Boro C and Xu R 2003 *Science* **301** 1078

[25] McQueeney R J, Lawson A C, Migliori A, Kelley T M, Fultz B, Ramos M, Martinez B, Lashley J C and Vogel S C 2004 *Phys. Rev. Lett.* **92** 146401

[26] Söderlind P, Kotliar G, Haule K, Oppeneer and Guillaumont D 2010 *MRS Bull.* **35** p. 883

[27] Johnson R A 1973 *J. Phys.* F: *Metal Phys.* **3** 295

[28] Baskes M I and Melius C F 1979 *Phys. Rev.* B **20** 3197

[29] Valone S M, Baskes M I and Martin R L 2002 *LA-UR-02-1958* (Los Almos National Laboratory)

[30] Dremov V, Sapozhnikov P, Kutepov A, Anisimov V, Korotin M, Shorikov A, Preston D L and Zocher M A 2008 *Phys. Rev.* B **77** 224306

[31] Gesari S B, Pronsato M E and Juan A 2002 *Appl. Surf. Sci.* **187** 207

[32] Sutton A P and Balluffi R W 1995 *Interfaces in Crystalline Materials* (Oxford: Clarendon Press)

[33] Howe J M 1997 *Interfaces in Materials* (New York: John Wiley)

[34] Parrinello M and Rahman A 1980 *Phys. Rev. Lett.* **45** 1196

[35] Baskes M I and Vitek V 1985 *Met. Trans.* A **16** 1625

[36] Kurtz R J and Heinisch H L 2004 *J. Nucl. Mater.* **329–333** 1199

[37] Kimura A, Kasada R, Morishita K, Sugano R, Hasegawa A, Abe K, Yamamoto T, Matsui H, Yoshida N, Wirth B D and Rubia T D 2002 *J. Nucl. Mater.* **307–311** 521

[38] Dudarev S L, Semenov A A and Woo C H 2003 *Phys. Rev.* B **67** 094103

[39] Cottrell G A 2003 *Fus. Eng. Des.* **66–68** 253

[40] Trinkaus H, Singh B N and Victoria M 1996 *J. Nucl. Mater.* **233–237** 1089